GEOLOGY | THE GEOLOGICAL SOCIETY OF AMERICA®

https://doi.org/10.1130/G45527.1

Manuscript received 27 August 2018
Revised manuscript received 20 December 2018
Manuscript accepted 3 January 2019

Published online 29 January 2019

Reaction-induced embrittlement of the lower continental crust

Sarah Incel[1,2]*, Loïc Labrousse[3], Nadège Hilairet[4], Timm John[5], Julien Gasc[2], Feng Shi[6], Yanbin Wang[6], Torgeir B. Andersen[7], François Renard[1,8], Bjørn Jamtveit[1], and Alexandre Schubnel[2]

[1]Physics of Geological Processes, The Njord Centre, Department of Geosciences, University of Oslo, P.O. Box 1048, Blindern, 0316 Oslo, Norway

[2]Laboratoire de Géologie de l'ENS, PSL Research University, UMR8538 du CNRS, 24 Rue Lhomond, 75005 Paris, France

[3]CNRS-INSU, Institut des Sciences de la Terre Paris, ISTeP, UMR 7193, Sorbonne Université, 75005 Paris, France

[4]Université Lille, CNRS, INRA, ENSCL, UMR 8207 - UMET–Unité Matériaux et Transformations, F-59000 Lille, France

[5]Institute of Geological Sciences, Freie Universität Berlin, Malteserstrasse 74-100, 12249 Berlin, Germany

[6]Center for Advanced Radiation Sources, University of Chicago, Chicago, Illinois 60637, USA

[7]Centre for Earth Evolution and Dynamics, Department of Geosciences, University of Oslo, P.O. Box 1047, Blindern, 0316 Oslo, Norway

[8]Université Grenoble Alpes, Université Savoie Mont Blanc, CNRS, IRD, IFSTTAR, ISTerre, 38000 Grenoble, France

ABSTRACT

Field observations and geophysical data reveal a causal link between brittle seismic failure and eclogitization of the lower continental crust. We present results from experimental deformation of plagioclase-rich samples at eclogite-facies conditions and quantify the link between rock rheology and the kinetics of the eclogitization reactions. The deformation was ductile both in the absence of reaction and when the progress of eclogitization was fast compared to the imposed strain rate. However, when the reaction rate was relatively slow, the breakdown of plagioclase into nanocrystalline reaction products triggered embrittlement, highlighted by a high acoustic emission activity. Fluid-induced plagioclase breakdown under eclogite-facies conditions is an exothermic reaction accompanied by a negative change in solid volume. This is similar to other mineral transformations that are known to trigger transformational faulting. We demonstrate that mineral reactions lead to brittle deformation in situations where reaction rates are slow compared to the deformation rate.

INTRODUCTION

The mechanisms leading to brittle seismic failure in Earth's lower continental crust are still poorly understood. On the one hand, experimental studies reveal that plastic deformation should be dominant in plagioclase-rich rocks under granulite-facies conditions (<1 GPa and 973 K; Tullis and Yund, 1992) in the presence of water (Bürgmann and Dresen, 2008). On the other hand, field studies on lower-crustal rocks in Norway and geophysical data from the Himalaya–Tibetan Plateau reveal a strong coupling among seismicity, fluid infiltration, and eclogitization of the metastable lower continental crust (Austrheim and Boundy, 1994; Jackson et al., 2004; Lund et al., 2004; Hetényi et al., 2007; John et al., 2009; Jamtveit et al., 2018).

In this study, we used acoustic emissions to highlight the change in rheological behavior of granulite from dominantly plastic to mostly brittle while undergoing metamorphic transformation at eclogite-facies conditions in the presence of a hydrous fluid.

MATERIALS AND METHODS

A granulite from Holsnøy, southwestern Norway, was used as sample material. It mostly consisted of plagioclase (≈90 vol%) and minor amounts of epidote, sometimes intergrown with alkali feldspar, spinel, corundum, clinopyroxene, amphibole, biotite, kyanite, garnet, and magnetite, which together made up the remaining 10 vol% (Fig. DR1 in the GSA Data Repository[1]). The sample was crushed and sieved to a grain size of <38 µm. This powder was washed using distilled water to remove the dust fraction, dried in an oven, and then left at ambient air humidity conditions. The same starting material was used for all experimental runs. The deformation experiments were conducted using the D-DIA apparatus (Wang et al., 2003), a deformation multi-anvil press, at the GeoSoilEnviro-CARS (GSECARS [Consortium for Advanced Radiation Sources]) beamline 13 BM-D of the Advanced Photon Source, Argonne National Laboratory, Illinois, USA. The D-DIA is equipped with an acoustic emission setup. The experimental setup has been explained in detail by Gasc et al. (2011) and Schubnel et al. (2013). Synchrotron X-ray radiographs as well as powder diffraction patterns were acquired every 5 min, respectively, to monitor the strain and the differential stress of the sample during the experimental run, at in situ pressure-temperature (*P-T*) conditions. Experimental conditions are summarized in the table in Figure 1. Details on the stress and strain calculation as well as on the analytical methods are given in the Data Repository.

RESULTS

Based on a comparison of the overall stress-strain evolution together with the records of acoustic emissions during the four experimental runs, three different mechanical behaviors can be distinguished. Differential stress continuously increased during the deformation of sample NG_2.5_1023 (constant *T*), which exhibited the highest strength and the least detected number of acoustic emissions (Figs. DR2A and DR2C). We refer to this behavior as strong and ductile. For sample NG_2.5_1173 (constant *T*),

*E-mail: s.h.m.incel@geo.uio.no

[1]GSA Data Repository item 2019087, details on stress and strain calculations, analytical methods, and activation energy calculation; and Figures DR1–DR5, is available online at http://www.geosociety.org/datarepository/2019/, or on request from editing@geosociety.org.

CITATION: Incel, S., et al., 2019, Reaction-induced embrittlement of the lower continental crust: Geology, v. 47, p. 235–238, https://doi.org/10.1130/G45527.1

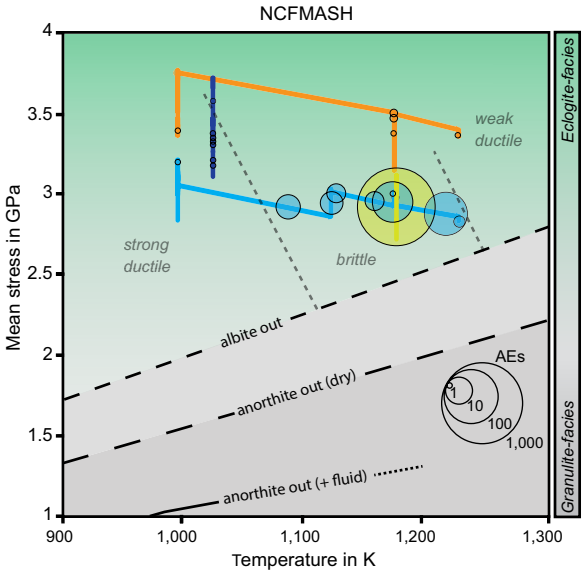

Sample	P_c in GPa	T in K	ε in %	$\dot{\varepsilon}$ in s^{-1}	# AEs	X in vol.%
NG_2.5_1023	2.5	1,023±50	35	5×10^{-5}	7	<1
NG_2.5_1173	2.5	1,173±50	37	6×10^{-5}	794	2.5
NG_2.5_1225	2.5	(995-1,225)±50	34	5×10^{-5}	82	5
NG_3_1225	3	(995-1,225)±50	36	5×10^{-5}	9	10

Figure 1. Mean stress-temperature curves on pressure-temperature (*P-T*) phase diagram showing stability of plagioclase and experimental conditions (table), where P_c = confining pressure; *T* = temperature; ε = finite strain; $\dot{\varepsilon}$ = strain rate; *X* = reacted plagioclase volume. AEs—acoustic emissions.

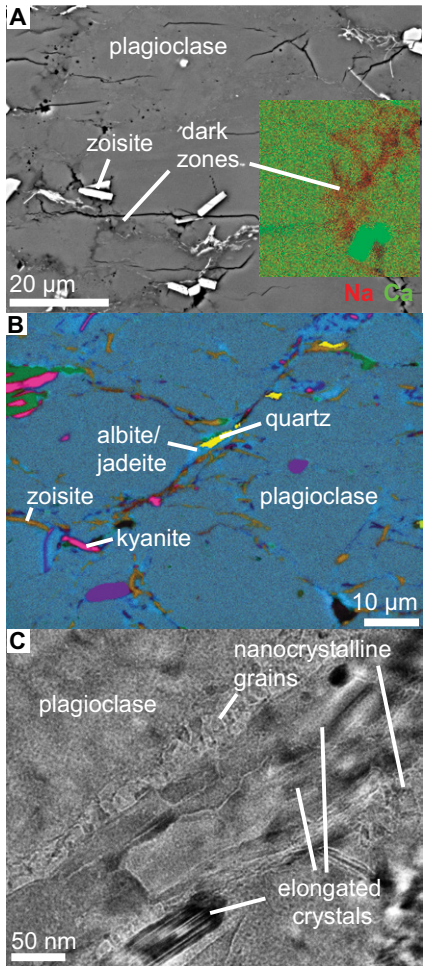

Figure 2. A: Backscattered electron (BSE) image with superimposed composite energy-dispersive X-ray spectroscopy (EDS) elemental map showing Ca and Na distribution. B: Composite EDS elemental map of area marked in Figure DR3H (see footnote 1). Bright bands in microstructure are composed of zoisite + kyanite + quartz ± albite ± jadeite. C: Transmission electron microscope (TEM) image, taken in bright field mode, showing cross-sectional view of selected bright band composed of elongated crystals with borders of isometrically shaped crystals. Location of this image is shown in Figure DR5 in the Data Repository. Maximum stress is vertical on images A and B.

the differential stress first increased to a peak stress of ~1.8 GPa at ~15% axial strain and then remained approximately constant until the end of deformation. In total, 794 acoustic emissions were recorded during deformation, and so this sample was in the brittle regime. Samples NG_2.5_1225 and NG_3_1225 both exhibited stress increase to ~2.3 GPa, followed by a large stress drop at ~14% axial strain. Their stress drop correlated with an imposed increase in temperature and did not coincide with the onset of acoustic emissions (dashed vertical lines in Fig. DR2). These samples showed a large variation in the total number of acoustic emissions: 82 for sample NG_2.5_1225 and only 9 for NG_3_1225. Sample NG_2.5_1225 clearly showed ample evidence for brittle deformation, while sample NG_3_1225 was weak and ductile (Figs. DR2A and DR2C). Figure 1 shows the calculated evolution in mean stress, $\sigma_m = (\sigma_1 + 2\sigma_3)/3$, with temperature. All samples were deformed under eclogite-facies conditions outside the plagioclase stability field (Fig. 1; De Capitani and Petrakakis, 2010). The samples deformed furthest from the plagioclase stability field produced the fewest acoustic emissions (Fig. 1).

Two main microstructural features appeared in the samples after deformation. Backscattered electron (BSE) images show dark areas in the plagioclase matrix indicative of a local difference in chemical composition (Fig. 2A). Another feature is the appearance of bands that are brighter than the adjacent plagioclase matrix in BSE mode (Fig. 3G). Both features, the dark areas and the bright bands, are very small (often <1 μm) and seem to be composed of different phases (Fig. 2B; Fig. DR3D). This makes precise measurements very difficult. However, energy-dispersive X-ray spectroscopy (EDS) analyses and semiquantitative element distribution maps were acquired with the scanning electron microscope (SEM) to compare the chemical compositions between the plagioclase matrix and these features. The dark zones were enriched in Na and depleted in Ca relative to the plagioclase matrix, suggesting a chemical composition close to albite or jadeite (Fig. 2A). Those zones were prominent in sample NG_2.5_1173 and mostly contained nanocrystalline grains (Figs. DR3D and DR4B). The bright crystals, which were most frequent in NG_3_1225, were mainly composed of elongated zoisite needles together with kyanite, quartz, and albite/jadeite (Figs. 2B and 2C). The location and abundance of both features within each sample were spatially correlated, but their respective amounts differed between samples (Fig. 3; Fig. DR3). The dark zones were prominent in sample NG_2.5_1173 (Fig. 2A) and rare in sample NG_3_1225, which mostly showed bright band-forming crystals (Fig. 2B). Sample NG_2.5_1225 showed both features in equal amounts (Figs. 3E and 3F).

DISCUSSION AND CONCLUSION

Both the bright bands and the dark areas reflect the onset of eclogitization by plagioclase breakdown in the presence of a hydrous fluid according to the reaction: plagioclase + fluid ↔ zoisite + kyanite + quartz ± $(NaSiCa_{-1}Al_{-1})_{plagioclase}$ ± jadeite (modified after Wayte et al., 1989). First, zoisite nucleates and grows, followed by the other product phases, which start to nucleate and grow at a more advanced plagioclase-transformation stage of ~10 vol% (Wayte et al., 1989). Reaction progress was estimated based on image analysis of the area fraction of the reaction products. Since kyanite and quartz were only found in sample NG_3_1225, this sample showed the highest degree of eclogitization, i.e., the highest reacted plagioclase volume, estimated to be ~10 vol% (Wayte et al., 1989). With respect to NG_3_1225, the other samples showed lower reacted plagioclase volumes of ~5 vol% for NG_2.5_1225, ~2.5 vol% for NG_2.5_1173, and less than 1 vol% for NG_2.5_1023 (Fig. 3). It is likely that water from ambient air humidity was adsorbed onto the grain surfaces during

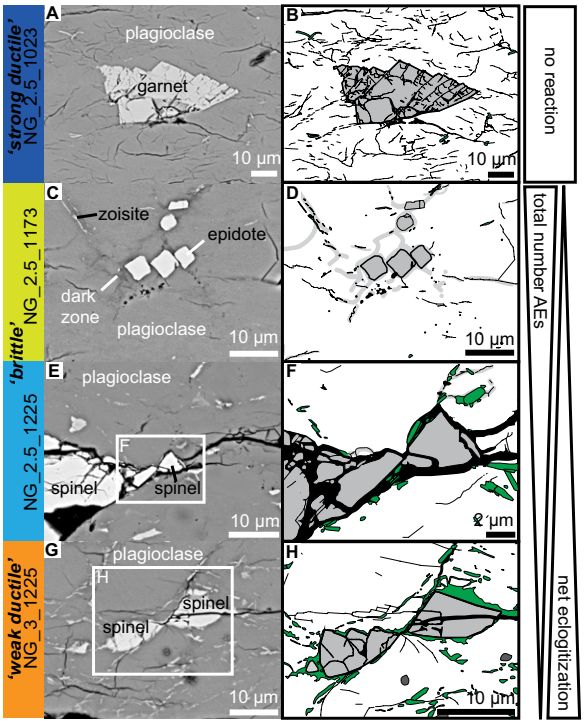

Figure 3. Backscattered electron (BSE) images of the four samples (A, C, E, G) with corresponding sketches (B, D, F, H). Maximum stress is vertical. Net eclogitization is deduced from abundance of eclogite-facies minerals with zoisite as a proxy (green areas in B, D, F, H). NG_2.5_1023 shows almost no reaction and is strong and ductile (A, B). Sample NG_2.5_1173 shows a low net eclogitization rate and is brittle (C, D). Although net eclogitization rate in sample NG_2.5_1225 is higher compared to sample NG_2.5_1173, this sample is also brittle (E, F), because amount of soft eclogite is not sufficient to dominate overall rheological behavior. Sample NG_3_1225 shows weak and ductile behavior, and its net eclogitization rate is high (G, H). AEs—acoustic emissions.

sample preparation, thus providing a possible fluid source to produce the hydrous phase zoisite. Another possible fluid source could be the plagioclase itself, since it can contain minor amounts of water in its crystal structure. Although small amounts of fluid are available during deformation, the overall reaction kinetics are expected to be sluggish, because they involve two successive processes. First, plagioclase is highly metastable (Fig. 1), and its breakdown will occur very rapidly as soon as it comes into contact with even low amounts of water. Second, the nucleation and growth of the reaction products are expected to be slower, because they involve chemical transport over longer distances. It is therefore reasonable to assume that the net rate of eclogitization is controlled by the nucleation and growth of the reaction products.

In a reacting rock, strain can be accommodated by transformation-induced volume changes. An imposed strain rate, $\dot{\varepsilon}$, can be expressed as the sum of a transformational strain rate, $\dot{\varepsilon}_t$, and a residual strain rate, $\dot{\varepsilon}_r$, with $\dot{\varepsilon} = \dot{\varepsilon}_t + \dot{\varepsilon}_r$. In this study, three scenarios can be deduced (Fig.3): (1) almost no reaction (NG_2.5_1023), (2) slow net eclogitization (NG_2.5_1225 and NG_2.5_1173), and (3) fast net eclogitization (NG_3_1225). If no or little deformation is accommodated by transformation reactions, the granulite is strong and ductile, and the microstructure of the sample shows distributed microcracks (Figs.3A and 3B), which trigger few acoustic emissions. If deformation can be partly accommodated by reaction and the net eclogitization is slow, the granulite samples show brittle behavior (Figs.3C–3F). Their microstructures contain partially eclogitized domains of nanocrystalline material (Figs.2A and 3C–3F).The residual strain, $\dot{\varepsilon}_r$, concentrates in these zones, which are weaker than the host granulite, eventually leading to brittle failure accompanied by acoustic emissions. In contrast, when the net eclogitization is fast, the sample is weak and ductile (Figs. 3G and 3H). Its microstructure and nanostructure contain numerous eclogite bands filled with oriented crystals (Figs. 2B and 2C), which enable sliding during further deformation. Because the mineral transformation kinetics depend on metastability (distance to equilibrium), plagioclase breakdown proceeded faster in sample NG_3_1225 than in sample NG_2.5_1225, deformed at a lower confining pressure. In conclusion, embrittlement is triggered by plagioclase breakdown, but as eclogite formation progresses, the overall rheological behavior of the sample becomes controlled by the soft eclogite. This has also been observed on Holsnøy, where unreacted and undeformed strong granulite blocks are embedded within a matrix of weak and deformed eclogite (Austrheim, 1990).

Eclogitization in nature, e.g., on Holsnøy, took place at $\dot{\varepsilon}$ and T values significantly lower than in our experiments. Assuming that the observed embrittlement is controlled solely by the rate of plagioclase breakdown relative to the imposed $\dot{\varepsilon}$, we can scale our laboratory conditions to those expected for natural systems. As a first-order approximation, $\dot{\varepsilon}_t$ can be expressed as:

$$\dot{\varepsilon}_t = \Delta V/V \times (d/d_o)^2 \times k_o \times exp^{-E_a/RT}. \quad (1)$$

This equation combines the volume change of the plagioclase breakdown reaction $\Delta V/V$ and the grain-size dependence on transformation progress, where d_o is the initial grain size, and d is the grain size after a certain amount of reaction with an Arrhenius-type T-dependence of the transformation rate ($k_o \times exp^{-E_a/RT}$). The parameters k_o, E_a, and R are the reaction rate constant, the activation energy, and the gas constant, respectively (see the Data Repository for further details on the calculation of E_a). Assuming that the reaction extent required to cause embrittlement in the laboratory is similar to that in nature, the laboratory transformational strain rate, $\dot{\varepsilon}_{t,lab}$, and the natural transformational strain rates, $\dot{\varepsilon}_{t,nat}$, are related by:

$$\dot{\varepsilon}_{t,lab}/\dot{\varepsilon}_{t,nat} = (d_{0,nat})/d_{0,lab})^2 \times exp[E_a/R \times (1/T_{nat} - 1/T_{lab})], \quad (2)$$

where T_{nat} is the eclogitization temperature on Holsnøy (~973 K; Raimbourg et al., 2005), and T_{lab} is the temperature under which embrittlement is observed in our experiments (~1173 K). The initial natural grain size $d_{o,nat}$ is ~1–3 × 10^{-3} m, and the initial laboratory grain size $d_{o,lab}$ is ~1–38 × 10^{-6} m. Figure 4 shows how the transformational strain rate ratio ($\dot{\varepsilon}_{t,lab}/\dot{\varepsilon}_{t,nat}$) required to cause brittle behavior varies with T. The onset of embrittlement would be expected at imposed natural strain rates, $\dot{\varepsilon}_{nat}$, of ~$10^{-9.8}$ s^{-1} (horizontal solid red line in Fig. 4), if the grain-size ratio is minimal $(d_{0,nat}/d_{0,lab})^2_{min}$ (solid black line in Fig. 4). However, assuming a maximal initial grain-size ratio $(d_{0,nat}/d_{0,lab})^2_{max}$ (dashed black line in Fig. 4) yields even lower imposed natural strain rates of $\dot{\varepsilon}_{nat}$ ~$10^{-13.8}$ s^{-1} (horizontal dashed red line in Fig. 4).

Previous experiments on the germanium - olivine-spinel transition (Burnley et al., 1991) showed a change in rheology similar to that presented in this study. Both transformations, plagioclase breakdown and olivine-spinel transition (Kirby et al., 1996), involve a negative volume change of ~14%–17% and 3%–10% and an exothermic latent heat release of ~10–13 kJ mol^{-1} and 10–50 kJ mol^{-1}, respectively. These thermodynamic properties probably play an important role in triggering brittle instabilities, as the negative volume change enables stress concentrations at crack tips (Kirby, 1987). Along with the heat released during the exothermic reactions, which would promote reactions to proceed even in the absence of larger amounts of fluid, these key ingredients may lead to the generation of self-localizing transformational faults. We show that, contrary to previous arguments (Kirby et al., 1996), transformational faulting is not limited to the case of polymorphic reactions.

Our results demonstrate that reaction-induced grain-size reduction together with a negative volume change trigger embrittlement in the laboratory. This is in accordance with findings of previous numerical and experimental studies on various lithologies (Burnley et al., 1991; Thielmann et al., 2015; Incel et al., 2017) and highlights embrittlement in the lower continental crust, at intermediate depth or deep in

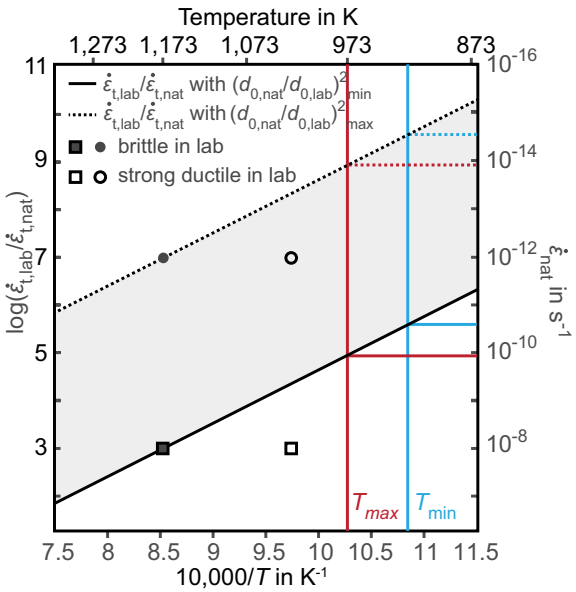

Figure 4. Arrhenius plot showing log ($\dot{\varepsilon}_{t,lab}/\dot{\varepsilon}_{t,nat}$) (laboratory transformational strain rate and natural transformational strain rate) versus 10,000/T. Vertical lines represent estimated maximum (red) and minimum (blue) eclogitization temperature on Holsnøy, Norway. Depending on initial grain-size ratio, $d_{o,nat}/d_{o,lab}$, required imposed natural strain rate ($\dot{\varepsilon}_{nat}$) for embrittlement is ~$10^{-9.8}$ to $10^{-13.8}$ s^{-1} (solid and dashed red horizontal lines).

Earth's mantle by the same underlying mechanism. It should be noted, however, that the reaction-driven embrittlement mechanism studied here requires a local fluid source. Otherwise, there will be no reaction. In our experiments, there was a small amount of fluid available for hydration reactions. For the Holsnøy case, fluids were introduced into an initially dry lower crust by lower-crustal earthquakes. Earthquakes in the lower crust prior to hydration may be triggered through stress pulses from earthquakes in the normal seismogenic regime (i.e., as aftershocks; Jamtveit et al., 2018). Incipient eclogitization reactions would then allow further brittle deformation in the wall rocks of earthquake-generated faults. In the case of the subducting Indian lower crust, deep crustal earthquakes have been interpreted to have been triggered by dehydration-produced fluids derived from the crust itself (Hetényi et al., 2007), in which case, reaction-driven embrittlement may even explain the initial earthquake activity.

ACKNOWLEDGMENTS

We thank Neil Mancktelow and the other anonymous reviewers who helped to improve the manuscript, as well as Damien Deldicque for the micro- and nanostructural analyses. The study received funding from the Alexander von Humboldt-Foundation (Feodor Lynen Research Fellowship to Incel). Further funding came from the People Program (Marie Curie Actions) of the European Union's Seventh Framework Program FP7/2017–2013/ and Horizon 2020 under REA grant agreements 604713 (to Schubnel) and 669972 (to Jamtveit), National Research Foundation Centre of Excellence grant 223272 (to Andersen), and National Science Foundation grant EAR-1661489 for the development of acoustic emission experiments (to Wang). This research used resources of the Advanced Photon Source, a U.S. Department of Energy Office of Science User Facility operated by Argonne National Laboratory (contract no. DE-AC02–06CH11357).

REFERENCES CITED

Austrheim, H., 1990, The granulite-eclogite facies transition: A comparison of experimental work and a natural occurrence in the Bergen arcs, western Norway: Lithos, v. 25, p. 163–169, https://doi.org/10.1016/0024-4937(90)90012-P.

Austrheim, H., and Boundy, T.M., 1994, Pseudotachylytes generated during seismic faulting and eclogitization of the deep crust: Science, v. 265, p. 82–83, https://doi.org/10.1126/science.265.5168.82.

Bürgmann, R., and Dresen, G., 2008, Rheology of the lower crust and upper mantle: Evidence from rock mechanics, geodesy, and field observations: Annual Review of Earth and Planetary Sciences, v. 36, p. 531–567, https://doi.org/10.1146/annurev.earth.36.031207.124326.

Burnley, P.C., Green, H.W., and Prior, D.J., 1991, Faulting associated with the olivine to spinel transformation in Mg_2GeO_4 and its implications for deep-focus earthquakes: Journal of Geophysical Research, v. 96, p. 425–443, https://doi.org/10.1029/90JB01937.

De Capitani, C., and Petrakakis, K., 2010, The computation of equilibrium assemblage diagrams with Theriak/Domino software: The American Mineralogist, v. 95, p. 1006–1016, https://doi.org/10.2138/am.2010.3354.

Gasc, J., Schubnel, A., Brunet, F., Guillon, S., Mueller, H.J., and Lathe, C., 2011, Simultaneous acoustic emissions monitoring and synchrotron X-ray diffraction at high pressure and temperature: Calibration and application to serpentinite dehydration: Physics of the Earth and Planetary Interiors, v. 189, p. 121–133, https://doi.org/10.1016/j.pepi.2011.08.003.

Hetényi, G., Cattin, R., Brunet, F., Bollinger, L., Vergne, J., Nábělek, J.L., and Diament, M., 2007, Density distribution of the India plate beneath the Tibetan Plateau: Geophysical and petrological constraints on the kinetics of lower-crustal eclogitization: Earth and Planetary Science Letters, v. 264, p. 226–244, https://doi.org/10.1016/j.epsl.2007.09.036.

Incel, S., Hilairet, N., Labrousse, L., John, T., Deldicque, D., Ferrand, T.P., Wang, Y., Morales, L., and Schubnel, A., 2017, Laboratory earthquakes triggered during eclogitization of lawsonite-bearing blueschist: Earth and Planetary Science Letters, v. 459, p. 320–331, https://doi.org/10.1016/j.epsl.2016.11.047.

Jackson, J.A., Austrheim, H., McKenzie, D., and Priestley, K., 2004, Metastability, mechanical strength, and the support of mountain belts: Geology, v. 32, p. 625–628, https://doi.org/10.1130/G20397.1.

Jamtveit, B., Ben-Zion, Y., Renard, F., and Austrheim, H., 2018, Earthquake-induced transformation of the lower crust: Nature, v. 556, p. 487–491, https://doi.org/10.1038/s41586-018-0045-y.

John, T., Medvedev, S., Rüpke, L.H., Andersen, T.B., Podladchikov, Y.Y., and Austrheim, H., 2009, Generation of intermediate-depth earthquakes by self-localizing thermal runaway: Nature Geoscience, v. 2, p. 137–140, https://doi.org/10.1038/ngeo419.

Kirby, S.H., 1987, Localized polymorphic phase transformations in high-pressure faults and applications to the physical mechanism of deep earthquakes: Journal of Geophysical Research–Solid Earth, v. 92, p. 13,789–13,800, https://doi.org/10.1029/JB092iB13p13789.

Kirby, S.H., Stein, S., Okal, E.A., and Rubie, D.C., 1996, Metastable mantle phase transformations and deep earthquakes in subducting oceanic lithosphere: Reviews of Geophysics, v. 34, p. 261–306, https://doi.org/10.1029/96RG01050.

Lund, M.G., Austrheim, H., and Erambert, M., 2004, Earthquakes in the deep continental crust—Insights from studies on exhumed high-pressure rocks: Geophysical Journal International, v. 158, p. 569–576, https://doi.org/10.1111/j.1365-246X.2004.02368.x.

Raimbourg, H., Jolivet, L., Labrousse, L., Leroy, Y., and Avigad, D., 2005, Kinematics of syneclogite deformation in the Bergen arcs, Norway: Implications for exhumation mechanisms, *in* Gapais, D., et al., eds., Deformation Mechanisms, Rheology and Tectonics: From Minerals to the Lithosphere: Geological Society of London Special Publication 243, p. 175–192, https://doi.org/10.1144/GSL.SP.2005.243.01.13.

Schubnel, A., Brunet, F., Hilairet, N., Gasc, J., Wang, Y., and Green, H.W., 2013, Deep-focus earthquake analogs recorded at high pressure and temperature in the laboratory: Science, v. 341, p. 1377–1380, https://doi.org/10.1126/science.1240206.

Thielmann, M., Rozel, A., Kaus, B.J.P., and Ricard, Y., 2015, Intermediate-depth earthquake generation and shear zone formation caused by grain size reduction and shear heating: Geology, v. 43, p. 791–794, https://doi.org/10.1130/G36864.1.

Tullis, J., and Yund, R., 1992, The brittle-ductile transition in feldspar aggregates: An experimental study: International Geophysics, v. 51, p. 89–117, https://doi.org/10.1016/S0074-6142(08)62816-8.

Wang, Y., Durham, W.B., Getting, I.C., and Weidner, D.J., 2003, The deformation-DIA: A new apparatus for high temperature triaxial deformation to pressures up to 15 GPa: The Review of Scientific Instruments, v. 74, p. 3002–3011, https://doi.org/10.1063/1.1570948.

Wayte, G.J., Worden, R.H., Rubie, D.C., and Droop, G.T.R., 1989, A TEM study of disequilibrium plagioclase breakdown at high pressure: The role of infiltrating fluid: Contributions to Mineralogy and Petrology, v. 101, p. 426–437, https://doi.org/10.1007/BF00372216.

Printed in USA